Developmental Cell, Vol. 1, 139–153, July, 2001, Copyright ©2001 by Cell Press

KDEL-Cargo Regulates Interactions between Proteins Involved in COPI Vesicle Traffic: Measurements in Living Cells Using FRET

Irina Majoul,[1] Martin Straub,[2] Stefan W. Hell,[2] Rainer Duden,[3] and Hans-Dieter Söling[1,4]
[1] Department of Neurobiology
[2] High Resolution Optical Microscopy Group
Max-Planck-Institute of Biophysical Chemistry
D-37077 Göttingen
Germany
[3] University of Cambridge
Wellcome Trust Centre for Molecular Mechanisms in Disease
Cambridge CB2 2XY
United Kingdom

Summary

How the occupied KDEL receptor ERD2 is sorted into COPI vesicles for Golgi-to-ER transport is largely unknown. Here, interactions between proteins of the COPI transport machinery occurring during a "wave" of transport of a KDEL ligand were studied in living cells. FRET between CFP and YFP fusion proteins was measured by multifocal multiphoton microscopy and bulk-cell spectrofluorimetry. Ligand binding induces oligomerization of ERD2 and recruitment of ARFGAP to the Golgi, where the $(ERD2)_n$/ARFGAP complex interacts with membrane-bound ARF1. During KDEL ligand transport, interactions of ERD2 with β-COP and p23 decrease and the proteins segregate. Both p24a and p23 interact with ARF1, but only p24 interacts with ARFGAP. These findings suggest a model for how cargo-induced oligomerization of ERD2 regulates its sorting into COPI-coated buds.

Introduction

Retrograde Golgi-to-ER transport by COPI-coated vesicles serves the continuous recycling of escaped ER resident proteins such as protein disulfide isomerase or BiP, which carry the carboxy-terminal retrieval signal -KDEL in mammals or -HDEL in yeast (Pelham, 1991; Letourneur et al., 1994; Wieland and Harter, 1999; Barlowe, 2000). This signal is recognized by the KDEL receptor ERD2, a protein mainly localized to the cis-Golgi, which targets its ligands into the retrograde COPI-mediated transport pathway (Semenza et al., 1990; Pelham, 1991; Griffiths et al., 1994). The ERD2-ligand complex returns to the ER where it dissociates, thus freeing ERD2 for further rounds of transport. The minimal machinery for the budding of COPI vesicles from Golgi membranes or liposomes in vitro consists of the small GTPase ARF1 in its GTP-bound form and the coat precursor complex, coatomer (Rothman and Wieland, 1996; Spang et al., 1998). In vivo, formation of COPI-coated vesicles from the Golgi involves additional factors: ARF1-specific GTPase-activating proteins (ARFGAPs), ARF1-GDP/GTP exchange factors, and members of the p24 protein family (reviewed in Donaldson and Jackson, 2000; Reinhard et al., 1999). An open question is whether cargo proteins also contribute to this process.

ARF1-GTP binds to Golgi membranes and recruits coatomer. This initial set of protein-protein interactions triggers the deformation of the membrane and the budding of COPI vesicles (reviewed in Rothman and Wieland, 1996; Bremser et al., 1999). A Golgi-localized ARFGAP is necessary for ARF1 function (Cukierman et al., 1995; Poon et al., 1999). ARFGAP-regulated GTP hydrolysis is required for the uncoating of COPI vesicles near the target membrane, but also for cargo inclusion during the budding of COPI-coated vesicles (Tanigawa et al., 1993; Lanoix et al., 1999; Nickel et al., 1998; Malsam et al., 1999; reviewed in Springer et al., 1999). In vitro coatomer can dramatically enhance ARFGAP-induced GTP hydrolysis by a soluble, N-terminally truncated form of ARF1, ΔN17-ARF1 (Goldberg, 1999). This action of coatomer can be inhibited in vitro by cytoplasmic tail peptides of p24a, but not of p23 or p24d (Goldberg, 2000). p24 proteins, which constitute a conserved family of type I transmembrane proteins in mammals and in yeast, are abundant constituents of COPII- and COPI-coated vesicles. They have been implicated in coat recruitment via their cytoplasmic tails. It has been proposed that these proteins function as cargo receptors through their lumenal domains. p24 family proteins can form heterooligomers, which cycle between the Golgi and the ER (Nickel et al., 1997; Füllekrug et al., 1999; Gommel et al., 1999; Blum et al., 1999). In *S. cerevisiae*, a disruption of all eight genes coding for p24 proteins has no effect on viability and is associated only with minor secretory defects, whereas mice with a p23 gene knockout die early in embryogenesis (Springer et al., 2000; Denzel et al., 2000). Thus, the function of p24 proteins is currently controversial.

Cargo proteins will need to interact with some of these components to be efficiently sorted into the budding COPI-coated vesicles or tubular structures. This should apply in particular to the ligand-occupied KDEL receptor ERD2, as binding of ligands to ERD2 stimulates its rapid transport out of the cis-Golgi (Lewis and Pelham, 1992; Hsu et al., 1992; Majoul et al., 1998). Townsley et al. (1993) were the first to consider ligand-induced conformational changes and/or oligomerization of ERD2 as a prerequisite for its retrograde transport to the ER. Indeed, Aoe et al. provided evidence by coimmunoprecipitation that either ERD2 overexpression or increased ligand binding to ERD2 enhances its homooligomerization and its association with ARFGAP (Aoe et al., 1997, 1998).

These observations led us to ask the following: (1) how, in the live cell, does ligand-induced ERD2 oligomerization lead to sorting of the occupied ERD2 for retrograde transport, and (2) how are other proteins of the machinery (ARFGAP, ARF1, COPI proteins, and p24 proteins) involved in this process in live cells?

To answer these questions, we have used as a model KDEL protein the A subunit of the nontoxic cholera toxin

[4] Correspondence: hsoelin@gwdg.de

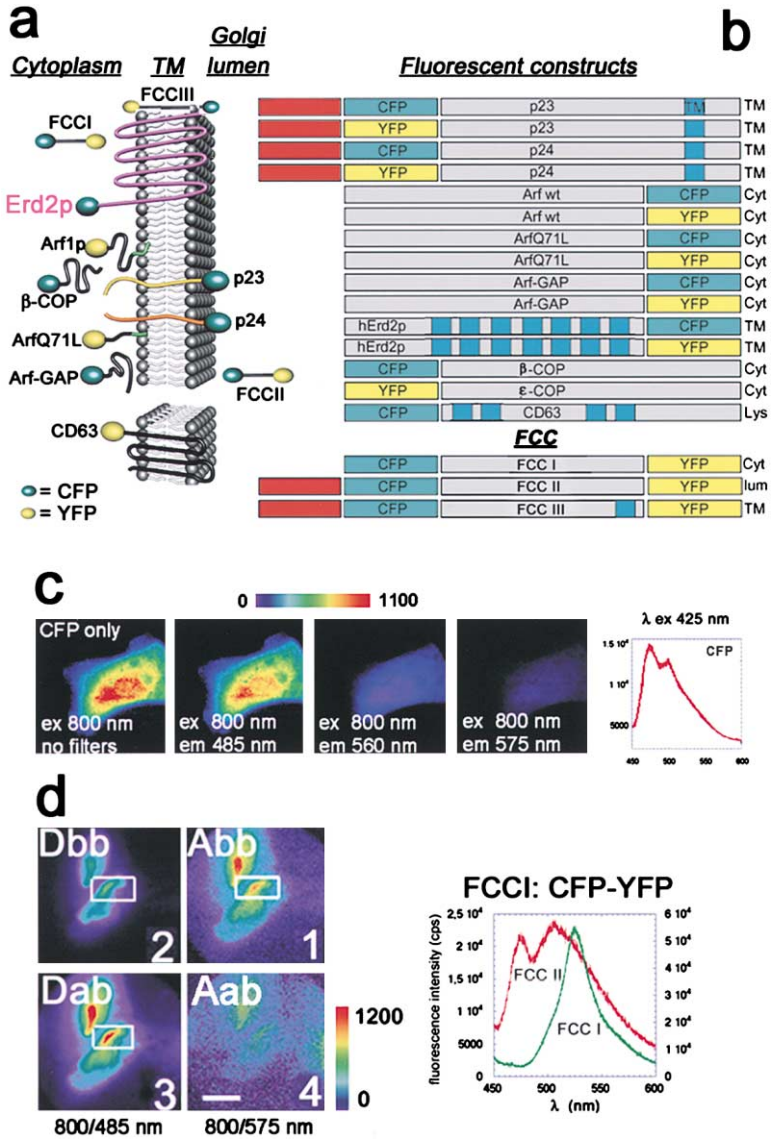

Figure 1. Constructed Fusion Proteins; FRET in Living Cells with Control Proteins FCC I and FCC II

(A) CFP and YFP fusion proteins and their Golgi membrane orientation. Proteins were expressed as CFP and YFP fusion proteins. FCC I is the cytoplasmic, FCC II the secretory cleavable, and FCC III the transmembrane control construct. CD63 is a lysosomal/endosomal protein.

(B) Fusion constructs used. Signal sequences are in red, transmembrane domains in blue, CFP moieties in blue-green, and YFP moieties in yellow. Not drawn to scale.

(C) Left panels: low overflow of CFP fluorescence into the YFP channel during excitation in the two-photon mode. Cells only overexpressing CFP were excited at 800 nm, and total fluorescence (no filters) and fluorescence at λ_{em} = 485 nm, 560 nm, and 575 nm was registered. Right panel: bulk-cell experiment showing the CFP emission spectrum (λ_{ex} = 425 nm).

(D) Left panel: intramolecular FRET between the CFP and YFP components of the secretory FCC II fusion protein measured by MMM. D_{bb}: donor fluorescence (λ_{ex} = 800 nm, λ_{em} = 485 nm) before bleaching; A_{bb}: acceptor fluorescence (λ_{ex} = 800 nm, λ_{em} = 575 nm) before acceptor bleaching for 3 min with 530 nm laser light; D_{ab}: donor fluorescence after bleaching; A_{ab}: acceptor fluorescence after bleaching. The mean D_{ab}/D_{bb} ratio was 1.68 ± 0.24 (range 1.42–2.01; n = 5). Right panel: bulk-cell spectrofluorimetry of cells expressing for 6 hr the cytoplasmic protein FCC I (green curve) or the secretory protein FCC II (red curve); λ_{ex} = 425 nm. Sensitized emission (at 526 nm) resulting from YFP excitation due to FRET for FCC I. FCC II shows in addition a peak at 474 nm resulting from partial cleavage of FCC II.

mutant CTX-K63 (Fontana et al., 1995), which can gain access to ERD2 from the outside of the cell (Majoul et al., 1996, 1998). Fluorescence resonance energy transfer (FRET) between pairs of fusion proteins tagged with spectrally shifted mutants of the green fluorescent protein, namely ECFP and EYFP, was measured in live Vero cells in the absence and presence of the external KDEL ligand. FRET between CFP and YFP fusion proteins was imaged as sensitized emission in single cells by multifocal multiphoton microscopy (MMM; Bewersdorf et al., 1998; Straub and Hell, 1998), allowing observation of the same intact cell over a time course of up to 2 hr. Multiphoton excitation with infrared light (λ_{ex} = 800 nm) is very benign to living cells (Denk and Svoboda, 1997). It confines imaging to a micron-thin plane, yielding a much higher contrast of the area of interest. Multifocality (see Experimental Procedures) reduces photostress further. The results obtained with these techniques allow us to propose a model for how KDEL cargo proteins can regulate their own sorting and transport.

Results

Testing the Reliability of FRET Measurements to Study Interactions of Proteins Involved in COPI-Dependent Transport in Live Cells

In single-cell experiments, FRET was verified by measuring the increase of donor fluorescence following bleaching of the acceptor, and expressed as the ratio of donor fluorescence after acceptor bleaching divided by donor fluorescence before acceptor bleaching (D_{ab}/D_{bb}). The wavelength settings applied in the MMM mode were selected such that during excitation at 800 nm, only a very low overflow of CFP fluorescence into the YFP channel occurred (Figure 1C). Our experimental system was tested by expressing FRET control proteins (FCC I and FCC II; see Figures 1A and 1B) in which CFP and YFP were separated by a short stretch of amino acids. Due to the small distance, a strong FRET between CFP and YFP should occur in live cells expressing these proteins. Cells expressing FCC II indeed exhibited a

clear FRET signal, which was verified by a strong increase of the bleaching ratio D_{ab}/D_{bb} (Figure 1D, left). FRET was also indicated by sensitized emission measured by spectrofluorimetry in bulk-cell experiments (Figure 1D, right). The FRET signal of expressed FCC I remained constant over the observation time (up to 120 min), indicating that cleavage did not occur. FCC II, which contained a proteolytic cleavage site for Golgi-resident protease, initially exhibited a similar degree of FRET as FCC I, but ~6 hr after transfection, a measurable portion of FCC II had become cleaved as seen from the appearance of a CFP peak (Figure 1D, right).

We expressed pairs of functionally unrelated fusion proteins as negative FRET controls. We chose the combinations CD63, a endosomal/lysosomal tetraspanin protein (Kobayashi et al., 2000) and ERD2, and CD63 and p23 (see supplemental Figures S1A and S1B at http://www.developmentalcell.com/cgi/content/full/1/1/139/DC1). Neither in the absence nor in the presence of the KDEL ligand CTX-K63 did the coexpressed pair ERD2-CFP/CD63-YFP show a spectral shift (spectrofluorimetry) or significant FRET signals in the MMM mode (mean D_{ab}/D_{bb} ratio 0.98 $\pm$ 0.07 [n = 6]). The same holds for the pair p23-CFP/CD63-YFP (mean D_{ab}/D_{bb} ratio 0.99 $\pm$ 0.01 [n = 4]). Furthermore, pairs of Golgi-localized proteins, namely p23-CFP/ARFGAP-YFP or Erd2-CFP/ARF1-YFP in the absence of the KDEL ligand CTX-K63, or p23-CFP/ERD2-YFP after CTX-K63, also did not exhibit FRET. The results indicate that FRET signals measured under our conditions result from specific protein-protein interactions. The D_{ab}/D_{bb} ratio is a very sensitive parameter for FRET. In experiments with cells coexpressing different pairs of noninteracting CFP and YFP fusion proteins, the D_{ab}/D_{bb} ratio never exceeded a value of 1.05 (n = 28).

Protein Interactions in the Budding Complex: Binding of KDEL Ligand to ERD2 Enhances its Oligomerization in the Live Cell

Coexpressed ERD2-CFP and ERD2-YFP exhibited an exact colocalization (Figure 2A). Moreover, when analyzed no later than 6–8 hr after transfection, the distribution of the ERD2 fusion proteins was very similar to that of the endogenous wild-type ERD2 (data not shown). When analyzed 6 hr after transfection, the internalized KDEL ligand CTX-K63 induced a transient increase in FRET between ERD2-CFP and ERD2-YFP in single-cell experiments (Figure 2B). Dequenching of donor fluorescence after acceptor bleaching indicated in each case that the measured sensitized emission had indeed resulted from FRET (Figure 2D). CTX-K63 also induced a time-dependent FRET increase between ERD2-CFP and ERD2-YFP when measured by spectrofluorimetry in bulk-cell experiments (Figure 2E).

At the time point of maximal coupling between ERD2-CFP and ERD2-YFP, we also observed a significant transmembrane FRET signal between ERD2-CFP and the Cy3-labeled KDEL ligand CTX-A-K63 subunit (Figure 2C). Cy3-labeled CTX-B subunit, which is rapidly taken up by the cells but does not possess a C-terminal KDEL signal, does not induce FRET between ERD2-CFP and Cy3-CTX-B (data not shown). These results indicate clearly that an increased binding of KDEL proteins to ERD2 induces its homooligomerization in the live cell.

An Interaction between ARFGAP and ERD2 Is Enhanced by the KDEL Ligand

Aoe et al. (1997) have shown by a coimmunoprecipitation approach that ERD2 can interact with an ARF GTPase-activating protein (ARFGAP). But does such an interaction also take place in the live cell, and if so, is it affected by increased ligand binding to ERD2? Under conditions of moderate overexpression of ERD2-CFP (up to 6 hr after transfection), the KDEL ligand CTX-K63 induced a strong interaction between ARFGAP-CFP and ERD2-YFP 30–60 min after the start of CTX-K63 uptake, as indicated by an increase in sensitized emission in single-cell experiments (Figure 3A) and by a strong donor dequenching after acceptor bleaching (Figure 3B). This occurred particularly in perinuclear areas, which showed accumulation of CTX-K63-A subunits (Figures 3E and 3F). Results were confirmed by bulk-cell experiments (Figures 3C and 3D). Increased FRET was followed by a decrease between 60 and 90 min (Figures 3A and 3D). Thus, under physiological conditions, ligand binding to ERD2 induces the recruitment of ARFGAP from the cytosol to the Golgi, most likely as a consequence of increased ERD2 oligomerization. This is followed by dispersion of ARFGAP together with ERD2 from the Golgi (Figure 3F, panels 2–5).

The KDEL Ligand Induces Interaction between ERD2 and ARF1

As binding of KDEL ligands to ERD2 induced its interaction with ARFGAP (see Figure 3), we next analyzed whether ligand-activated ERD2 interacts with ARF1, either directly or within an ARFGAP/ARF1 complex. In the absence of CTX-K63, FRET between ARF1-CFP and ERD2-YFP was low or absent, both in single-cell and bulk-cell experiments (Figure 4A), but increased strongly 30–50 min after the start of CTX-K63 uptake (Figures 4B and 4C, lower panel). Thus, the binding of the KDEL ligand to ERD2 also induces an interaction between ERD2-YFP and ARF1-CFP.

Increased Interaction between ARF1 and ARFGAP following Ligand Binding to ERD2

Our results indicate the formation of a budding complex in the Golgi, which includes occupied oligomerized ERD2, ARF1, and ARFGAP. This is strongly supported by experiments with cells coexpressing ARF1-CFP and ARFGAP-YFP for no more than 5–6 hr; while FRET signals between the two fusion proteins were weak or absent before addition of the external KDEL ligand, strong FRET signals appeared in single-cell as well as bulk-cell experiments 40 min after the start of uptake of the external KDEL ligand (compare Figures 5A and 5B). After 120 min, FRET signals became weaker or disappeared (Figure 5C).

Ligand Binding to ERD2 Induces a Dispersion of ARFGAP But Not of ARF1 from the Golgi

Both ARF1-CFP and ARFGAP-YFP are expressed as soluble proteins and thus are present throughout the cytoplasm (Figures 3A, 4A, and 5A). However, ARF1-CFP is enriched on perinuclear structures already before

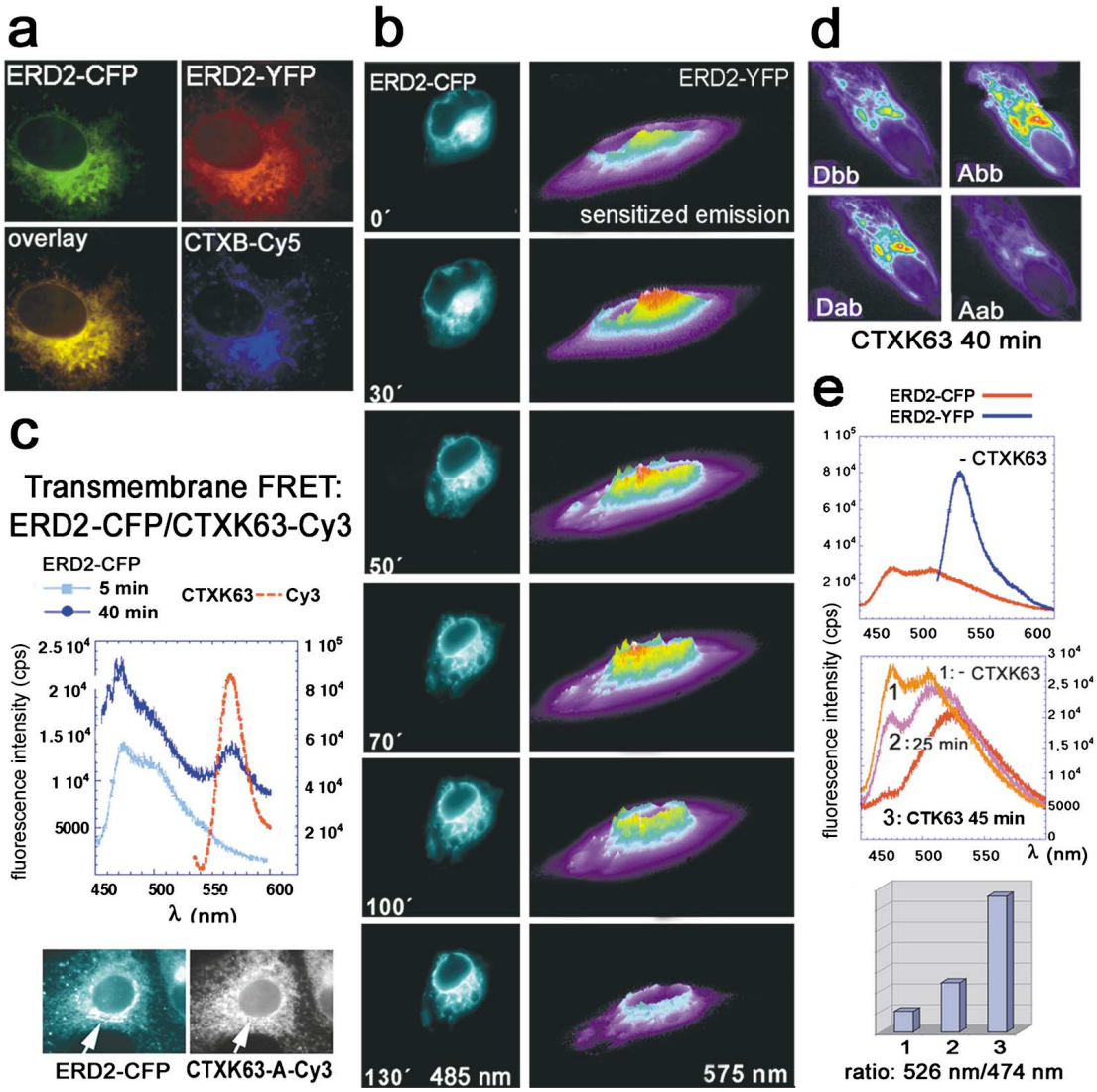

Figure 2. Binding of the KDEL Ligand CTX-K63 Induces FRET between ERD2-CFP and ERD2-YFP

(A) Colocalization of ERD2-CFP and ERD2-YFP 35 min after the start of CTX-K63 uptake. Note ERD2 dispersion and its partial colocalization with Cy5-CTX-K63.

(B) Right panels: time-dependent change of ERD2-YFP-sensitized emission after CTX-K63 uptake during two-photon excitation of ERD2-CFP. Left panels: ERD2 dispersion starts when sensitized emission increases (same cell as in the right panel, but only CFP emission was registered).

(C) Transmembrane FRET between ERD2-CFP and Cy3-labeled CTX-K63. Vero cells expressing ERD2-CFP were analyzed by spectrofluorimetry (λ_{ex} = 425 nm) 5 min (light blue curve) and 40 min (dark blue curve) after the start of uptake of Cy3-labeled CTX-K63. The peak at 560 nm, representing sensitized emission, is visible after 40 min but not after 5 min, and coincides with the maximum of the Cy3 emission spectrum obtained during excitation at λ_{ex} = 530 nm (red curve). Right panels: a cell from the same experiment showing the distribution of ERD2-CFP (upper cell) and Cy3-CTX-K63 (lower cell), 45 min after the start of Cy3-CTX-K63 uptake.

(D) FRET 40 min after the start of CTX-K63 uptake as confirmed by acceptor bleaching (single cell; MMM mode). A_{bb} and D_{bb}: acceptor and donor fluorescence before bleaching; A_{ab} and D_{ab}: acceptor and donor fluorescence after bleaching.

(E) CTX-K63-induced FRET measured as sensitized emission by spectrofluorimetry in cells coexpressing ERD2-CFP and ERD2-YFP. Cells from segments of a single plate were scraped off before or 25 or 40 min after the start of uptake of CTX-K63, suspended in PBS, and analyzed by measuring the spectrum of the excited fluorescence during excitation of the CFP moiety at λ_{ex} = 425 nm. Fluorescence was normalized to protein content of the samples. Upper left panel: CFP fluorescence spectrum (red curve) before CTX-K63 (λ_{ex} = 425 nm), and the same cells excited at λ = 498 nm representing YFP fluorescence (blue curve). Right panel: time-dependent red shift (sensitized emission) before (1) and at 25 min (2) and 40 min (3) after the start of CTX-K63 uptake (excitation at λ_{ex} = 425 nm). The time-dependent increase of the 526 nm/474 nm fluorescence intensity ratio is quantitated in the lower left panel.

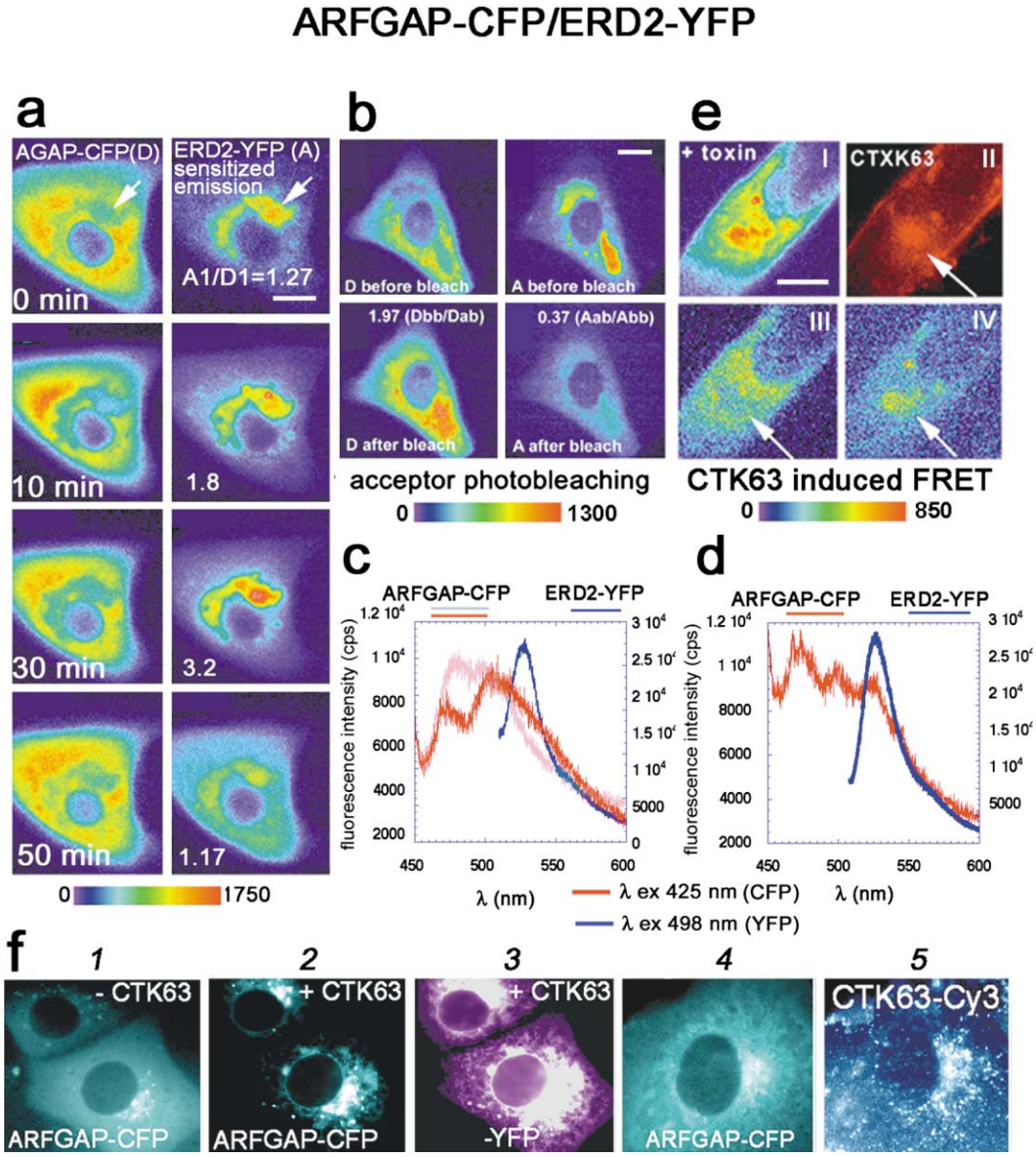

Figure 3. Time-Dependent FRET between ARFGAP-CFP and ERD2-YFP Induced by the KDEL Ligand (CTX-K63)

(A) Time course of CTX-K63-induced sensitized emission (MMM mode). The increase of the acceptor (A)/donor (D) fluorescence ratio from 1.27 to 3.2 is followed by a decrease.

(B) Bleaching control: enhanced acceptor fluorescence following CTX-K63 (35 min) analyzed in the two-photon mode before and after acceptor bleaching. A_{bb} and D_{bb}: acceptor and donor fluorescence before bleaching; D_{ab} and A_{ab}: acceptor and donor fluorescence after bleaching (bleaching ratio $D_{ab}/D_{bb} = 1.97$).

(C and D) Bulk-cell experiment with cells coexpressing ARFGAP-CFP and ERD2-YFP. Cells from the same plate analyzed ($\lambda_{ex} = 425$ nm) before (magenta curve in [C]), 40 min (red curve in [C]), and 100 min (red curve in [D]) after the start of CTX-K63 uptake. Blue curves represent the same cells, but excited at $\lambda_{ex} = 498$ nm. Representative of four similar experiments.

(E) FRET 30 min after the start of CTX-K63 uptake. Panel I: two-photon mode ($\lambda_{ex} = 800$ nm; unfiltered emission); panel II: Perinuclear and plasma membrane localization of Cy3-labeled CTX-K63 (xenon lamp; $\lambda_{ex} = 543$ nm, $\lambda_{em} = 560$ nm); panel III: two-photon mode, donor fluorescence; and panel IV: two-photon mode acceptor fluorescence. Localized loss of donor fluorescence in panel III (white arrow) colocalizes with increased acceptor fluorescence and CTX-K63 in panels IV and II, respectively. The scale bars in (A), (B), and (E) represent 10 μm.

(F) The external KDEL ligand induces recruitment of ARFGAP to and its subsequent dispersion from the Golgi. ARFGAP-CFP before the addition of CTX-K63 (panel 1), ARFGAP (panel 2), and ERD2-YFP (panel 3) 50 min after the start of CTX-K63 uptake. Panels 4 and 5 show ARFGAP and CTX-K63, respectively, in another cell.

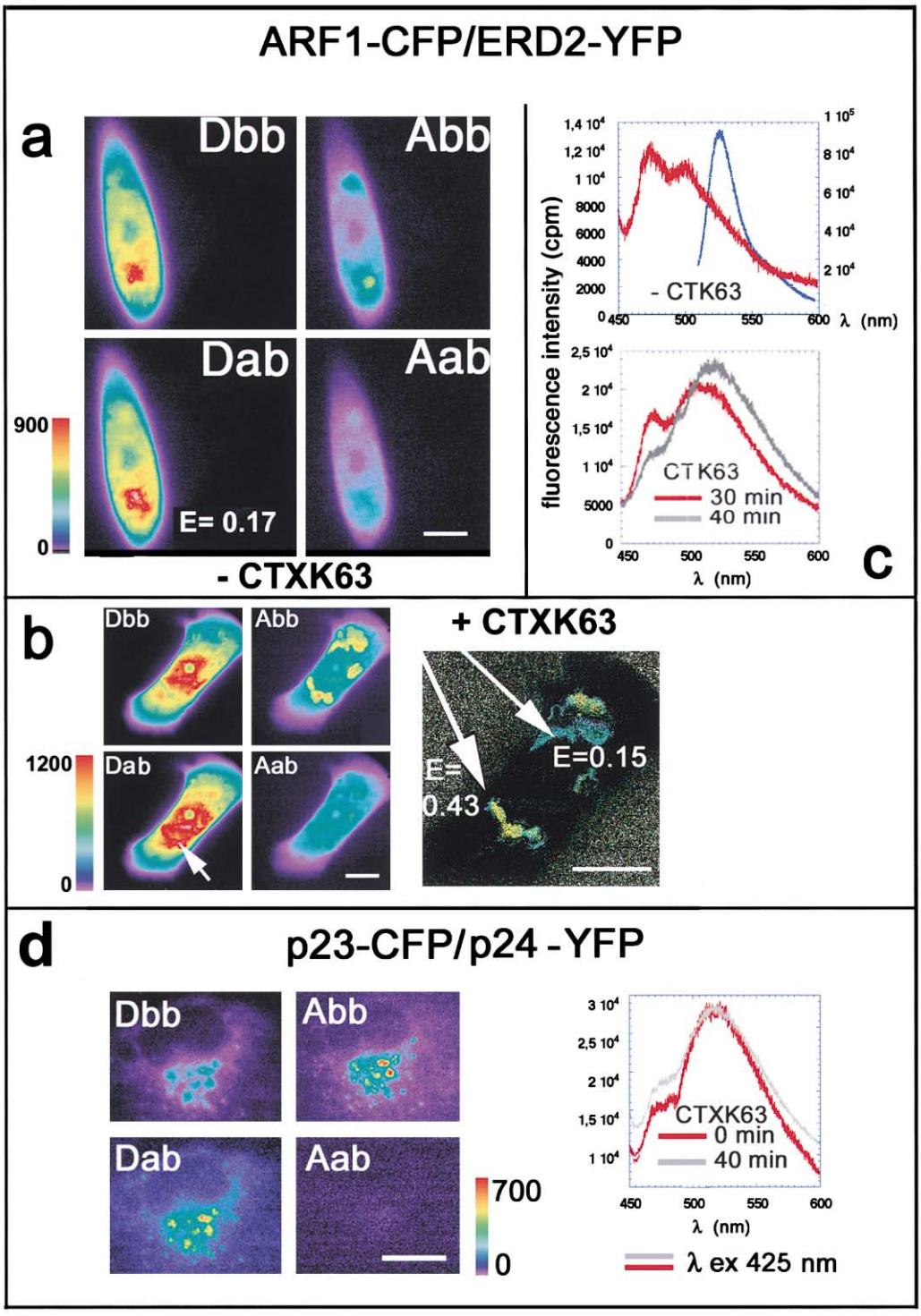

Figure 4. The KDEL Ligand CTX-K63 Enhances FRET between ARF1-CFP and ERD2-YFP without Affecting the Strong FRET between p23-CFP and p24a-YFP

(A) Moderate FRET between ARF1-CFP and ERD2-YFP in the absence of CTX-K63. A_{bb} and A_{ab}: acceptor fluorescence before and after bleaching; D_{bb} and D_{ab}: donor fluorescence before and after acceptor bleaching. The D_{ab}/D_{bb} ratio was 1.17. The scale bar represents 10 μm.

(B) Increased FRET (white arrow in panel D_{ab}) 30 min after the start of CTX-K63 uptake assessed by MMM. A_{bb} and A_{ab}: acceptor fluorescence before and after bleaching; D_{bb} and D_{ab}: donor fluorescence before and after acceptor bleaching. The D_{ab}/D_{bb} ratio increased from 0.97 ± 0.11 (n = 7) in the absence to 1.24 ± 0.22 (n = 28) in the presence of CTX ($p < 0.02$). E: FRET efficiency. The scale bar represents 10 μm.

(C) Bulk-cell experiment. FRET measured by spectrofluorimetry (λ_{ex} = 425 nm) in ARF1-CFP and ERD2-YFP coexpressing cells. Cells from the same plate analyzed immediately before (upper panel), and 30 and 40 min after the start of uptake of the KDEL ligand CTX-K63 (lower panel). Blue curve represents the peak of the YFP emission of the same cells during excitation at 498 nm. Two additional experiments gave similar results.

(D) Left panels: FRET between p23-CFP and p24a-YFP; single-cell experiment, MMM mode. A_{bb} and A_{ab}: acceptor fluorescence before and after bleaching; D_{bb} and D_{ab}: donor fluorescence before and after bleaching. In five separate experiments, the mean D_{ab}/D_{bb} ratio was elevated to 1.35 ± 0.20 (n = 5). The scale bar represents 10 μm. Right panel: bulk-cell experiment showing a strong sensitized emission (λ_{ex} = 425 nm). The position of the spectral peak corresponds to that of the YFP spectrum taken at λ_{ex} = 498 nm (blue curve in [C]). Cells from the same culture plate did not exhibit a decrease of sensitized emission 40 min after the start of CTX-K63 uptake (gray curve). Three additional experiments gave similar results.

exposure of the cells to the external KDEL ligand (Figures 4A, 5A, and 5D). This changes little after ligand-induced dispersion of the occupied ERD2. By contrast, ARFGAP is recruited to the Golgi mainly 15–40 min after the start of CTX-K63 uptake (Figures 3, 5B, and 5D), and starts to leave it again when ERD2 and the KDEL ligand disperse from the Golgi (Figure 3F, panels 4 and 5). From these data it can be concluded that during COPI-mediated retrograde transport, ARFGAP cycles between the cytoplasm and Golgi membranes, whereas ARF1 does not, or does so at a much slower rate.

p23-CFP and p24a-YFP Oligomerize in Live Cells

Coimmunoprecipitation experiments indicate that p24 proteins can interact with each other in the Golgi membrane (Dominguez et al., 1998; Gommel et al., 1999; Marzioch et al., 1999). In vitro binding experiments with the C-terminal, cytoplasmically oriented peptide of p23 and coatomer gave a stoichiometry of 4/1, indicating that homotetramers of p23 or heterotetramers of p23 and p24a may be involved in coatomer binding to the Golgi membrane (Reinhard et al., 1999). In cells coexpressing CFP and YFP fusion proteins of p23 and p24a, both N-terminally tagged proteins localized to the Golgi, similar to endogenous p23 or p24a. The FRET signal indicated an interaction between the two proteins in the live cell in single-cell and bulk-cell experiments (Figure 4D). CTX-K63 application did not change this interaction (Figure 4D, right panel). Thus, the heterotropic interaction between p24 family members observed in vitro also takes place in live cells, but is affected little during enhanced retrograde transport of occupied ERD2.

Measuring Transmembrane FRET between p23-CFP and Cytoplasmically Oriented YFP Proteins

For p23 and p24a, the CFP moiety had to be attached to the lumenally oriented N terminus to keep their functionality, whereas the CFP/YFP moieties of all other fusion proteins used in this study were cytoplasmic. Therefore, measuring interactions between p23-CFP and YFP fusion proteins located on the cytoplasmic side of the Golgi membrane required registration of transmembrane FRET. To test the feasibility of measuring trans-Golgi membrane FRET, we devised a transmembrane FRET control construct (FCC III, depicted in Figures 1A and 1B). It consists of the p23 signal peptide, a lumenally exposed N-terminal CFP moiety, the p23 protein including its transmembrane domain, and a cytoplasmically exposed YFP moiety close to the C terminus. At its C terminus, FCC III harbors the cytoplasmic tail of p23, which ensures a Golgi localization of FCC III. Upon expression in Vero cells, FRET between the CFP and YFP moieties of FCC III could indeed be measured by both MMM and spectrofluorimetry (Figure 6A), which is thus proof of principle for transmembrane FRET. The transmembrane orientation of expressed FCC III was verified by trypsin digestion in streptolysin O-permeabilized Vero cells, which led to an expected decrease of the molecular mass of FCC III from ~78 kDa to ~48 kDa, the mass of the transmembrane region plus the lumenal portion of FCC III (Figure 6A, middle panel). The 48 kDa cleavage product still reacted with an anti-GFP antibody, but no longer with antibodies directed against the cytoplasmic C terminus of p23. Trypsin digestion in the presence of Triton X-100 also removed the lumenal part of the protein as indicated by the loss of anti-GFP reactivity (Figure 6A, middle panel). Thus, transmembrane FRET can be registered in our experimental system.

Transmembrane FRET between p23-CFP and ERD2-YFP Is Affected by Binding of the KDEL Ligand CTX-K63 to ERD2

Single-cell (Figures 6B and 6C) and bulk-cell experiments (Figure 6E, panel A) revealed strong transmembrane FRET signals between p23-CFP and ERD2-YFP already before the addition of CTX-K63. This was followed by a further increase 30–40 min after the start of CTX-K63 uptake (Figure 6E, panel B). But after 90–120 min, when most of the model KDEL protein had arrived in the ER, FRET signals disappeared in single-cell (Figure 6D) and bulk-cell experiments (Figure 6E, panel C). This loss of interaction between p23 and ERD2 was accompanied by a visible segregation of these proteins (Figure 6F). Under these conditions, the KDEL ligand colocalized with ERD2, but no longer with p23 (Figure 6G).

ERD2 Interacts with Coatomer-Incorporated β-COP

Coatomer is involved in cargo selection during COPI vesicle budding (Gaynor et al., 1998; Wieland and Harter, 1999). Therefore, we tested whether an interaction between β-COP-CFP and ERD2-YFP might occur during sorting/transport of the oligomerized ERD2. The half-life of the COPI/coatomer complex is ~28 hours (Lowe and Kreis, 1996). In accordance with this, 4 hr after transfection, most of the β-COP-CFP was diffusely distributed in the cytoplasm and no FRET between β-COP-CFP and ERD2-YFP was observed (data not shown). However, 8–10 hours after transfection, a detectable amount of β-COP-CFP appeared in perinuclear structures colocalizing with ERD2-YFP, most likely representing cis-Golgi. In these structures, significant FRET signals indicated interactions of ERD2 with β-COP (Figure 7A), as was confirmed by bulk-cell experiments (Figure 7A, middle panel). These observations fit well with the colocalization of β-COP and ERD2 in retrograde COPI vesicles observed by immunoelectron microscopy by Orci et al. (1997). However, 60 min after the start of CTX-K63 uptake, the interaction between the two fusion proteins had almost completely disappeared (Figure 7A, right panel), most likely reflecting the uncoating process.

ARF1 Interacts with p23 and p24a

The appearance of FRET signals between p23 and ERD2 as well as between ARF1 and ERD2 (see Figure 3) indicated that p24 proteins ARF1 and ERD2 might exist together with coatomer in a tight budding complex. Here, we show in living cells that ARF1 is indeed closely associated with p23 or p24a, a possibility that had been

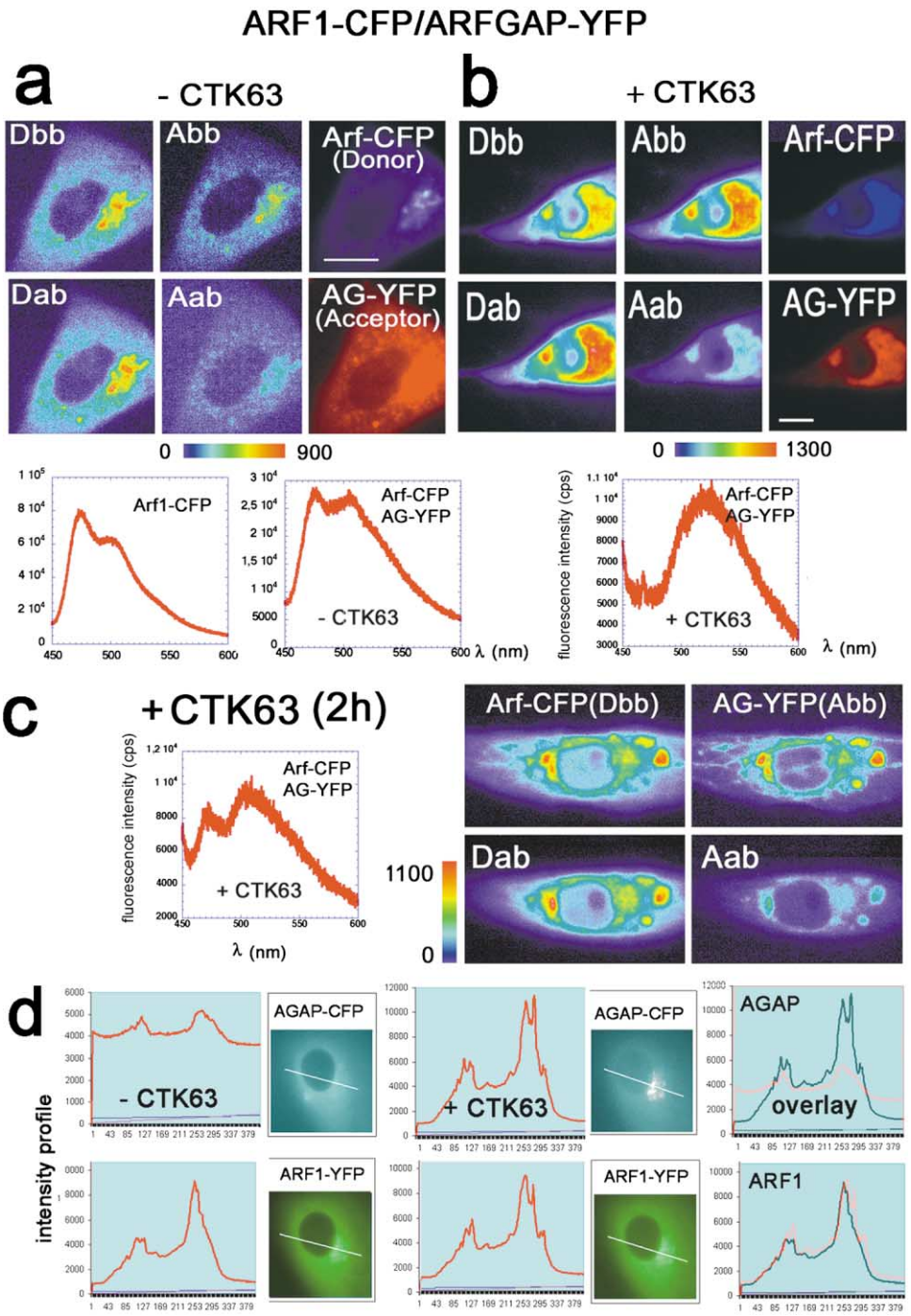

Figure 5. Ligand Binding to ERD2 Induces FRET between ARF1-CFP and ARFGAP-YFP

(A) Low or absent FRET between ARF1-CFP and ARFGAP-YFP in the absence of CTX-K63 measured in the MMM mode (left panels) or in bulk-cell experiments (right panels). Upper right panel: spectrofluorimetry of bulk cells expressing only ARF1-CFP. Lower right panel: bulk-cell experiment showing FRET between ARF1-CFP and ARFGAP-YFP in the absence of CTX-K63.

(B) FRET between ARF1-CFP and ARFGAP-YFP, 50 min after the start of uptake of the external KDEL ligand. Left panels: MMM measurement showing donor fluorescence after acceptor bleaching. Right panel: bulk-cell experiment.

(C) Decreased interaction between ARF1-CFP and ARFGAP-YFP, 120 min after the start of CTX-K63 uptake. Left panels: very low FRET signal as indicated by donor fluorescence following acceptor bleaching. Right panel: bulk-cell experiment. Reappearance of the ARF1-CFP peak at $\lambda = 474$ nm indicates that the association between ARF1 and ARFGAP has decreased (compare to [B]).

(D) CTX-K63 induces recruitment of ARFGAP to the Golgi. ARFGAP-CFP and ARF1-YFP coexpressed for 8 hr. The distribution of CFP (upper panels) and YFP fluorescence (lower panels) intensities across a cell was registered by a line scan before and 40 min after the start of CTX-K63 uptake.

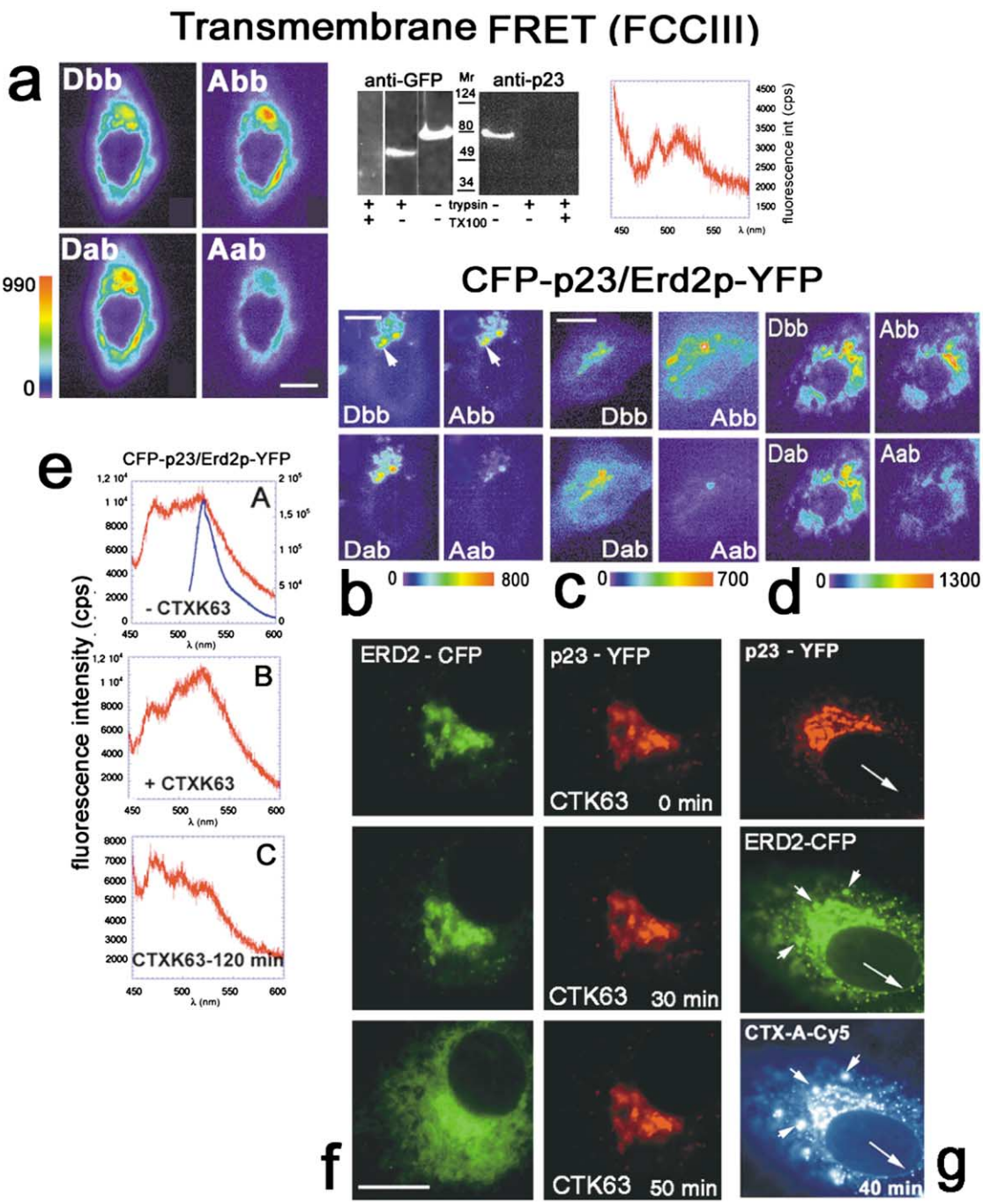

Figure 6. The External KDEL Ligand CTX-K63 Decreases FRET between p23-CFP and ERD2-YFP

(A) Control experiment using control construct III (FCC III; see Figures 1A and 1B) to demonstrate transmembrane FRET. Left panel: single-cell experiment, MMM mode; A_{bb} and A_{ab}: acceptor fluorescence before and after bleaching; D_{bb} and D_{ab}: donor fluorescence before and after bleaching. Middle panels: orientation of expressed FCC III in the Golgi membrane; trypsin digestion of FCC III in SLO-permeabilized Vero cells in the absence and presence of Triton X-100; immunostaining with antibodies against GFP (left) or the cytoplasmic tail of p23 (right). Right panel: spectrofluorimetry; cells expressing FCC III show transmembrane FRET as indicated by sensitized emission during excitation at $\lambda_{ex} = 425$ nm. The main peak coincides with the YFP emission peak (compare with blue emission curve in panel [E]).

(B and C) FRET between p23-CFP and ERD2-YFP in the absence of the KDEL ligand CTX-K63 measured in two single cells in the MMM mode. A_{bb} and A_{ab}: acceptor fluorescence before and after bleaching. D_{bb} and D_{ab}: donor fluorescence before and after bleaching. The mean D_{ab}/D_{bb} ratio from five separate single-cell MMM experiments was 1.30 $\pm$ 0.18. The scale bars in (A–C) represent 10 μm.

(D) As for (B) and (C), but 120 min after the start of CTX-K63 uptake. Note the loss of FRET and the segregation of p23-CFP (D_{bb}) and ERD2-YFP (A_{bb}). The mean D_{ab}/D_{bb} ratio from six separate experiments was 0.93 $\pm$ 0.06.

(E) Bulk-cell experiment. Cells expressing p23-CFP and ERD2-YFP were analyzed by spectrofluorimetry ($\lambda_{ex} = 425$ nm) before (panel A), 45 min (panel B), and 120 min (panel C) after the start of CTX-K63 uptake. Similar results were obtained in three additional experiments. Blue curve in panel A represents the emission spectrum taken at $\lambda_{ex} = 498$ nm showing the YFP component of ERD2-YFP.

(F and G) p23-YFP and Erd2-CFP segregate during the transport of the ERD2 ligand from the Golgi to the ER. Distribution of ERD2-CFP and p23-YFP in the same cell before and 30 and 50 min after the start of CTX-K63 uptake (F). p23-YFP, ERD2-CFP, and Cy5-labeled CTX-A-K63 in the same cell 40 min after the start of CTX-K63 uptake (G).

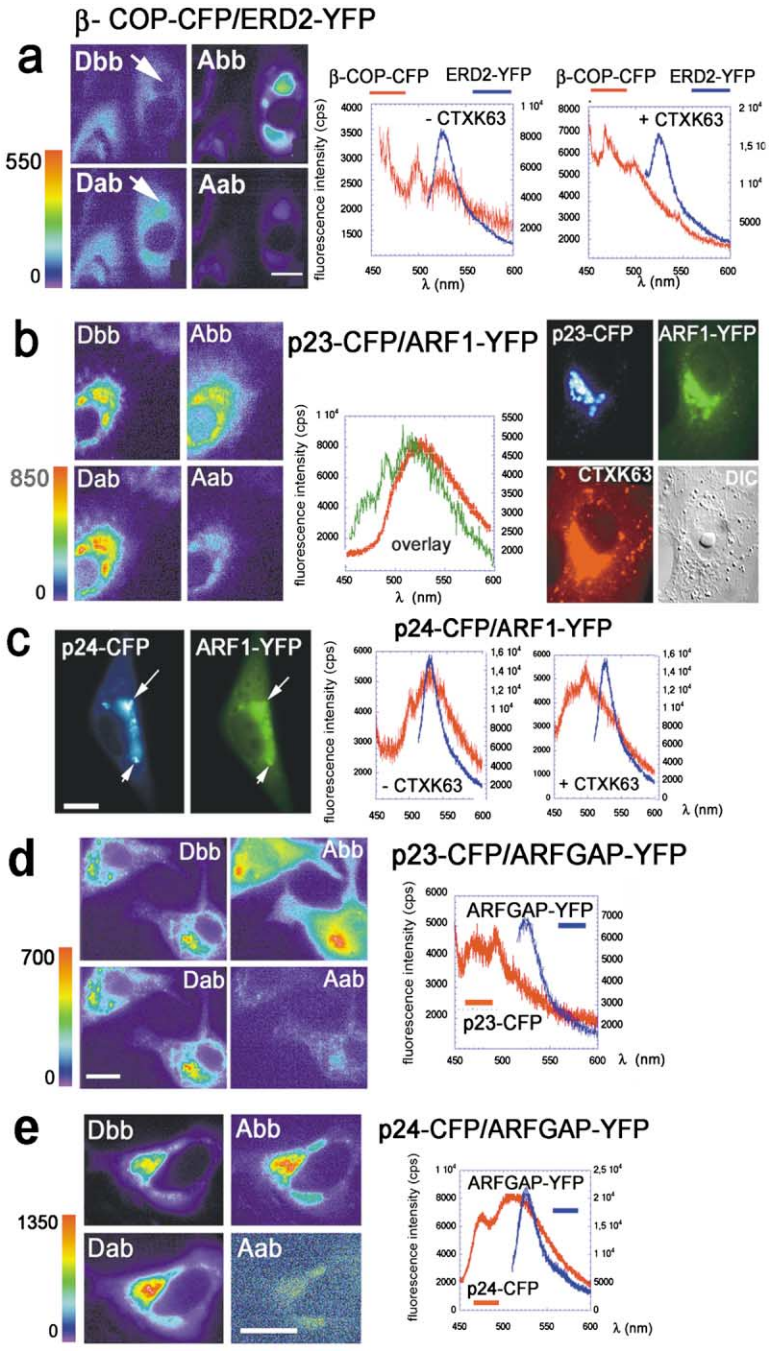

Figure 7. Binding of KDEL Ligand to ERD2 Decreases FRET between β-COP-CFP and ERD2-YFP, But Has Little Effect on FRET between p23-CFP or p24a-CFP and ARF1-YFP; ARFGAP-YFP Interacts with p24 But Not with p23

(A) Left panels: FRET between β-COP-CFP and ERD2-YFP in the absence of CTX-K63. MMM experiment with two neighboring cells; A_{bb} and A_{ab}: acceptor fluorescence before and after bleaching (only the right cell was bleached); D_{bb} and D_{ab}: donor fluorescence before and after bleaching. The mean D_{ab}/D_{bb} ratio was 1.49 ± 0.44 (n = 15) and exceeded a value of 1.2 in 10 out of the 15 experiments. Right panels: CTX-K63 leads to a FRET decrease between β-COP-CFP and ERD2-YFP (bulk-cell experiment; sensitized emission, λ_{ex} = 425 nm). Blue curves correspond to emission spectra taken at λ_{ex} = 498 nm representing ERD2-YFP. The scale bar represents 10 μm.

(B) p23-CFP interacts with ARF1-YFP in the absence and presence of CTX-K63. Left panels: single-cell MMM; D_{bb} and D_{ab}: donor before and after bleaching; A_{bb} and A_{ab}: acceptor before and after bleaching. The mean D_{ab}/D_{bb} ratio was 1.20 ± 0.10 (n = 5, range 1.08–1.36). Middle panel: bulk-cell experiment. Spectrofluorimetry showing FRET between p23-CFP and ARF1-YFP before (green curve) and after (red curve) the addition of CTX-K63 (λ_{ex} = 425 nm). Right panels: localization of Cy3-labeled CTX-K63, p23-CFP, and ARF1-YFP 50 min after the start of uptake of CTX-K63. DIC: differential interference contrast picture of the same cell.

(C) p24a-CFP interacts with ARF1-YFP in the absence and presence of CTX-K63. Left panels: colocalization of p24a-CFP and ARF1-YFP 60 min after the start of CTX-K63 uptake. Right panels: bulk-cell experiments. Sensitized emission (λ_{ex} = 425 nm) indicates FRET before the start of CTX-K63 uptake (− CTXK63; red curve) and 60 min after the start of CTX-K63 uptake (+ CTXK63; red curve). Two additional experiments gave almost identical results. Blue curves correspond to emission spectra taken at λ_{ex} = 498 nm representing ARF1-YFP. The scale bar represents 10 μm.

(D) Absence of significant FRET between p23-CFP and ARFGAP-YFP. Left panels: single-cell MMM bleaching experiment. A_{bb} and A_{ab}: acceptor before and after bleaching; D_{bb} and D_{ab}: donor before and after bleaching. The mean D_{ab}/D_{bb} ratio was 0.93 ± 0.06 (n = 6). Right panel: bulk-cell experiments, sensitized emission (red curve; λ_{ex} = 425 nm). Blue curve represents the spectrum of ARFGAP-YFP in the same cells taken at λ_{ex} = 498 nm. Representative of three similar experiments.

(E) Interaction between p24a-CFP and ARF-GAP-YFP. Left panels: interaction between p24a-CFP and ARF1-YFP (single-cell MMM). The mean D_{ab}/D_{bb} ratio was 1.30 ± 0.36 (n = 5; range 0.91–1.97; the ratio exceeded a value of 1.10 in four out of five experiments). Right panel: bulk-cell experiment. FRET between p24a-CFP and ARF1-YFP as indicated by sensitized emission during excitation at λ = 425 nm. Blue curve represents the emission spectrum of ARFGAP-YFP in the same cells when excited at λ = 498 nm. Representative of four similar experiments.

discussed recently by Wieland and Harter (1999). In the absence of the external KDEL ligand, both p24a-CFP and p23-CFP interacted with ARF1-YFP in bulk-cell and single-cell MMM experiments (Figures 7B and 7C). The D_{ab}/D_{bb} ratio was 1.32 ± 0.08 (n = 8) for p24a-CFP/ARF1-YFP and 1.20 ± 0.10 (n = 5) for p23-CFP/ARF1-YFP. FRET between p23 and ERD2 disappeared 60–120 min after the start of CTX-K63 uptake (Figure 6), but the association between p24a or p23 and ARF1 persisted (Figures 7B and 7C). This is underscored by the observation that Golgi-associated ARF1-YFP and p24a-CFP or p23-CFP colocalized up to 2 hr after the start of CTX-K63 uptake (Figures 7B and 7C), and that unlike ERD2 and the KDEL ligand, ARF1-YFP did not leave the Golgi

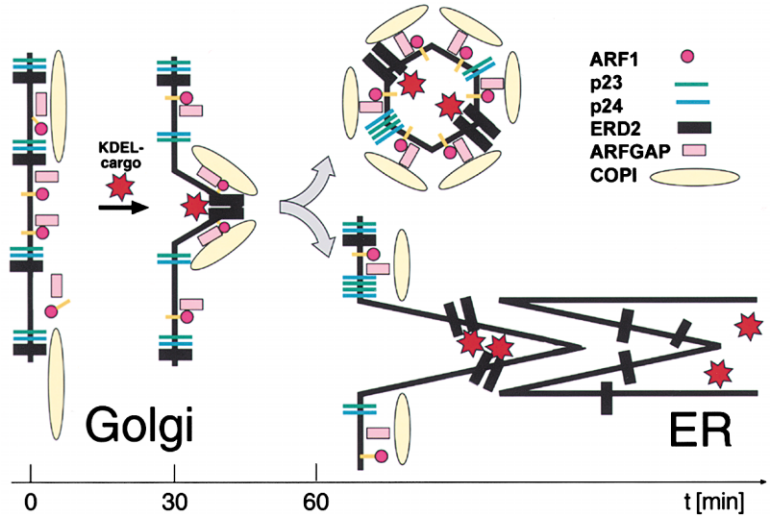

Figure 8. Model for KDEL Ligand-Induced Formation of a Budding Complex in the cis-Golgi

In the absence of a KDEL ligand the KDEL receptor ERD2 exists mainly in monomeric form, but most likely associated with coatomer and p23 or p23/p24a heterooligomers. A significant amount of ARF1, but much less ARFGAP, is associated with the Golgi membrane. Binding of a KDEL ligand to ERD2 leads to its oligomerization, which induces recruitment of ARFGAP to the Golgi membrane. $(ERD2)_n$ forms a complex with ARFGAP and ARF1 while still binding to coatomer and p23 homo- or p23/p24a heterooligomers. Formation of the complex, to which binding of p23/p24a to ARF1 further contributes, favors formation of buds into which ligand-bound ERD2 oligomers are sorted. Coated buds develop then either to COPI-coated vesicles (upper part) or to tubular extensions (lower part). After the release of ARFGAP and uncoating, COPI vesicles fuse with the ER membrane, whereas the uncoated tips of tubular extensions fuse temporarily with specific sites of the ER. The time scale refers to the time after the start of CTX-K63 uptake. To simplify the scheme, only free, nonoligomerized ERD2 is shown at time zero. In reality, recycling of endogenous KDEL proteins is always associated with a certain fraction of occupied, oligomerized ERD2.

(Figures 7B and 7C). Our data are compatible with a model in which ARF1 undergoes cycling between the GDP- and GTP-bound forms without leaving the membrane (Barlowe, 2000).

p24a-CFP, But Not p23-CFP, Interacts with ARFGAP-YFP

Under in vitro conditions using N-terminally truncated ARF1 and ARFGAP, coatomer enhanced ARFGAP activity >1000-fold (Goldberg, 2000). This coatomer effect was inhibited by the p24a, but not by the p23 or p24d cytoplasmic tail peptides, pointing to the possibility that p24a but not p23 interacts with ARFGAP. Our approach allowed us to address this question in intact cells. FRET signals for the pair p23-CFP/ARFGAP-YFP were very weak or absent when measured in single-cell or bulk-cell experiments (Figure 7D). This did not change in the presence of CTX-K63 (mean D_{ab}/D_{bb} ratio = 1.04 ± 0.11 [n = 6]).

By contrast, for the p24a-CFP/ARFGAP-YFP pair, a clear FRET signal was observed in single-cell experiments in the absence of CTX-K63 (Figure 7E). The mean D_{ab}/D_{bb} ratio was 1.30 ± 0.36 (range 0.91–1.97; the ratio exceeded a value of 1.10 in four out of five experiments). For the same pair, we also observed a strong sensitized emission in bulk-cell experiments (Figure 7E, right panel). Both results indicate a close association between p24a and ARFGAP. Thus, in agreement with Goldberg's in vitro findings, p23 and p24a display a remarkable difference concerning their association with ARFGAP in the intact cell.

p23 Binds to Wild-Type ARF1 But Not to ARF1-Q71L

Does p23 interact with ARF1 in its GTP- or its GDP-bound form? To address this question, we analyzed the interaction between p23 and ARF1-Q71L, an ARF1 mutant that exists mainly in the GTP-bound form (Dascher and Balch, 1994). FRET between p23-CFP and ARF1-Q71L-YFP was negligible (mean D_{ab}/D_{bb} ratio 1.03 ± 0.06 [n = 11]). This contrasts with the significant interaction between p23-CFP and ARF1-YFP (mean D_{ab}/D_{bb} ratio 1.20 ± 0.1 [n = 5]), and might thus indicate that p23 binds preferentially to ARF1 in its GDP-bound form. ARF1-Q71L-YFP used here was "functionally" active, as in cells coexpressing ARFGAP-CFP and ARF1-Q71L-YFP, a clear FRET signal was registered even in the absence of the external KDEL ligand (mean D_{ab}/D_{bb} ratio 1.22 ± 0.09 [n = 11]). Our data are in good agreement with in vitro results of D. Gommel, W. Nickel, and F.T. Wieland (personal communication), who also observed higher affinities of p23 for ARF1-GDP than for ARF1-GTP.

Discussion

FRET MMM Measurement in Living Cells and Demonstration of Transmembrane FRET

We have analyzed interactions between components of the COPI transport machinery that occur during a "wave" of transport of a model KDEL ligand. Several lines of evidence suggest that the interactions measured for various pairs of CFP/YFP fusion proteins are specific, and represent those of the corresponding wild-type proteins, as follows: (1) coexpressed CFP/YFP fusion proteins without functional connections did not give FRET signals; (2) under the conditions of moderate overexpression used in our experiments, the intracellular localization of the membrane proteins ERD2-CFP, ERD2-YFP, p23-CFP, and p24a-CFP was indistinguishable from that of the endogenous wild-type proteins; and (3) interactions described for some proteins (e.g., ERD2/ERD2 [Aoe et al., 1997], ERD2/ARFGAP [Aoe et al., 1997], and p23/p24a [Gommel et al., 1999]) using cell-destructive techniques were confirmed here in living cells. However, the strongest support for the physiological relevance of the interactions measured here comes from

the fact that most interactions were affected by a physiological trigger, namely the enhanced binding of a KDEL ligand to ERD2.

The transmembrane FRET shown here is compatible with theoretical considerations. The thickness of a phospholipid bilayer is 27–35 Å (Lewis and Engelman, 1983). On the basis of the length of the membrane spanning α-helical domains of Golgi enzymes (17 amino acids), Bretscher and Munro (1993) calculated the thickness of the Golgi membrane as $\sim$25.5 Å. Assuming the fluorophore domains of CFP and YFP are situated in the middle of a cylinder of about 4 nm in height and 2.5 nm in diameter (Tsien, 1998), the average distance between the membrane-separated fluorophores would be 25 Å + 2×12.5 Å = 50 Å. Under conditions of random tumbling of the CFP and YFP moieties (i.e., $\kappa^2 = 2/3$), the Förster radius amounts to $R_0 = 50.5$ Å (Tsien, 1998). The Golgi phospholipid membrane, due to its different refractive index, induces a reduction of the Förster radius of no more than 13% allowing for a FRET efficiency of 31% (for further details, see supplemental material).

FRET Signals Reveal Novel Interactions between Proteins of the COPI-Dependent Machinery and with Cargo

Our FRET measurements demonstrate that the binding of the ligand CTX-K63 induces ERD2 oligomerization. As the ligand also enhances FRET between ERD2-YFP and ARFGAP-CFP, it is likely that oligomeric ERD2 interacts with ARFGAP. Ligand binding to ERD2 also induces interactions between ERD2 and ARF1 and between ARF1 and ARFGAP, suggesting that the oligomerization of ERD2 contributes to the formation of a budding complex by bringing (ligand-ERD2)$_n$, ARF1, and ARFGAP into close proximity. This complex seems to be required for the sorting of the occupied, oligomerized ERD2 into COPI/coatomer coated buds, and may also favor ARFGAP-regulated hydrolysis of ARF1-bound GTP, which is required for effective cargo-sorting into COPI vesicles (Nickel et al., 1998; Lanoix et al., 1999; Malsam et al., 1999).

The "interaction" between p23 and ERD2 most likely results from an interaction of their transmembrane domains. Fiedler and Rothman (1997) observed that charged and polar amino acids in the transmembrane domain of p24 proteins are particularly important for their sorting. The latter is also true for the sorting of other transmembrane proteins, and we speculate that the seventh transmembrane spanning domain of ERD2 may be involved, as its aspartate 193 is highly conserved and indispensible for Golgi-ER translocation (Townsley et al., 1993). Consistent with in vitro data of Gommel et al. (1999), we detect a strong interaction between p23 and p24. This could potentially appear to conflict with our observation that p24a but not p23 interacts with ARFGAP. However, it is possible that ARFGAP interacts only with free or homooligomerized p24a, but not with free or homooligomerized p23. The preferential interaction of p24a with ARFGAP seems to be specific, as in cells coexpressing p23-CFP or p24-CFP with hGLO3-YFP, a novel human ARF-GAP implicated in the ER-Golgi transport cycle, neither p24a-CFP nor p23-CFP gave significant FRET signals in the absence or presence of the external KDEL ligand, even though hGLO3-CFP interacted with ERD2-YFP (I.M., G. Frigerio, S.W.H., H.-D.S., and R.D., unpublished data). Dominguez et al. (1998) observed that the cytoplasmic tail of p23 but not that of p24a binds coatomer, whereas both bind the COPII protein Sec23p. Previous studies have shown that the cytoplasmic tail of p23, but not that of p24, serves as a Golgi-ER retrieval signal (Nickel et al., 1997; Fiedler et al., 1996), and in studying the retrograde transport of the ERD2 ligand CTX-K63 from the Golgi to the ER, we observed an inhibition by anti-p23, but not by anti-p24a, antibodies (Majoul et al., 1998). Thus, our results further strengthen the notion that p23 and p24a are functionally distinct.

The cytoplasmic tails of p24 proteins and of ERD2 are so short that they are unlikely to interact with more than one other protein. However, as p24 proteins seem to exist mainly as tetramers (Reinhard et al., 1999), it seems possible that one p24a protomer interacts directly with ARF1 and a second with ARFGAP. Likewise, the interaction of ERD2 with β-COP and with ARF-GAP might be explained by assuming that one ERD2 subunit of an ERD2 dimer binds to ARFGAP, and the other to a coatomer component. Alternatively, in a tightly packed (ERD2)$_n$/ARFGAP/ARF1/coatomer complex, FRET between β-COP-CFP and ERD2-YFP could also occur without the direct binding of all components to each other.

Our data indicate that during the ARF1-GDP/ARF1-GTP cycle, most of ARF1 stays associated with the Golgi membrane due to interactions with membrane "receptor" proteins, such as p23. This would allow the GEF proteins to catalyze ARF1-GTP formation directly at the site where it is required. By contrast, ARFGAP leaves the Golgi membrane when most of the KDEL cargo has left the Golgi. So it seems to be ARFGAP, and not ARF1, which cycles between the cytosol and Golgi membrane during retrograde Golgi-ER transport.

Occupied ERD2 is transported all the way to the ER, but the majority of p23 is rapidly cycled back from the intermediate compartment or from tubular extensions of the cis-Golgi network. Under these circumstances, efflux of ERD2 out of the Golgi can become visible as "ERD2 dispersion" and at the same time can lead to segregation of ERD2 from p23 (Figure 6F). A tentative model of the protein-protein interactions taking place during the sorting of occupied ERD2 into COPI vesicles is depicted in Figure 8. Our data show that an increased load of KDEL cargo in the Golgi complex can stimulate its sorting into retrograde COPI vesicles. A physiological role of such a mechanism could clearly be to assist "ER quality control" (e.g., via the recycling of BiP and other KDEL proteins involved in this process), especially in situations of increased cellular stress (Hammond and Helenius, 1995).

Experimental Procedures

Microscope Setup

MMM experiments were carried out as described previously (Bewersdorf et al., 1998; see Supplemental Figures S1A and S1B) using a mode-locked titanium:sapphire laser (Mira 900-F, Coherent) providing 140 fs pulses at a repetition rate of 76 MHz with ~2 W average power (λ = 800 nm). The Ti:sapphire laser was pumped by a large frame Ar-Kr-Ionlaser (INNOVA 410, Coherent). The beam was expanded by a zoom telescope and passed through an edge filter (OG550, Schott), which removed residual emission in the visible spectrum. The beam then impinged onto a rotating microlens disk described elsewhere in detail (Bewersdorf et al., 1998; Straub and Hell, 1998). The microlenses were arranged in such a way that the beam was split into ~30 single beamlets that were transformed by the microscope into an array of high-resolution foci at the sample. An inverted Leica DM-IRB microscope was used as basic microscopic setup. Fluorescent light passed a dichroic mirror and was detected by a CCD Camera (UltraPix Si250, LSR AstroCam), or for real-time observations directly by eye. Images were recorded using an oil immersion objective (Leica PL APO, 100×, NA 1.4). In order to block reflections of laser light, a 3 mm BG39 filter (Schott) was placed in front of the camera. Additional band-pass and edge filters (see below) were used as emission filters. Cells were grown on coverslips and introduced into a temperature-controlled superfusion microscope chamber at 37°C for all MMM experiments (Straub et al., 2000).

FRET Measurements by MMM and In Situ Multifocal Bleaching

For an estimation of fluorescence intensity of CFP and YFP fusion proteins, images of the cells illuminated by the mercury lamp of the Leica DM-IRB (one-photon mode) were recorded before and subsequent to the MMM experiments (two-photon mode). For one-photon imaging for CFP, a 436/7 excitation filter was used in combination with a 485/20 band-pass emission filter, whereas YFP was excited through a 540/25 band-pass filter and detected with a 575 nm long-pass emission filter. For MMM FRET measurements, the CFP components of CFP fusion proteins were two-photon exited at 800 nm. Using the filter sets described, direct excitation of YFP by two-photon excitation at λ = 800 nm was negligible (<1.3% of fluorescence obtained during lamp excitation at λ = 520 nm). As FRET occurs only if the two corresponding fluorophores are within <6 nm, excitation of the CFP moiety (λ = 425 nm) should produce cyan fluorescent light (λ = 474 nm) when there is no YFP nearby, but a mixture of cyan and yellow light (λ = 526 nm) when there is. Bleaching of the YFP in a complex of CFP and YFP fusion proteins will return the emission to λ = 474 nm. FRET was estimated by comparing MMM images recorded with 485/20 band-pass and 575 nm long-pass filters immediately before and after bleaching of the live cell without any further readjustment of the sample. For bleaching, a second laser beam from an Ar-Kr ion laser (INNOVA 70C Spectrum, Coherent) at λ = 530 nm was coupled into the beam path. Its power was distributed such that 0.05 mW was applied in each of the ~30 foci. The wavelength λ = 530 nm ensured that CFP (maximum excitation: 440 nm) was bleached only negligibly, while more than 95% of the YFP (maximum excitation: 515 nm) was bleached within 3 min. The z position of the sample was held constant within ~100 nm as checked by a capacitive sensor. Samples that changed shape during bleaching were disregarded. FRET is expressed as the ratio D_{ab}/D_{bb} (D_{ab} and D_{bb} signify donor fluorescence intensity after or before acceptor bleaching, respectively). Time dependence of FRET was estimated in single-cell experiments from changes in sensitized emission (enhanced acceptor emission) upon two-photon excitation using the 575 nm long-pass filter, because dequenching of donor fluorescence following acceptor bleaching is not applicable under these conditions. The bleaching efficiency was determined by a comparison of the mercury lamp images of YFP fluorescence before and after bleaching. Sixteen bit images were acquired and processed to generate pseudocolor representations and quantitative data using MetaMorph (Universal Imaging) software. Mean values ± SD are given.

Fluorescence Spectrophotometry

Cells were washed with PBS, scraped from the plate, and suspended in 37°C warm PBS to a final concentration of ~5–15 × 10^7 cells/ml. Immediately thereafter, emission spectra of the cell suspensions were measured in a Fluoromax 2 spectrofluorimeter using excitation at 425 and 498 nm. FRET was estimated as sensitized emission of the YFP from the increase of the fluorescence intensity ratio 526 nm/474 nm upon excitation at λ_{ex} = 425 nm. Effects of cell sedimentation over the time needed to register a spectrum were negligible. For measuring effects of CTX-K63, the cell layer of a culture plate was divided into the appropriate number of segments. Cells from the first segment served as untreated controls and were prepared for spectrofluorimetry as given above. Subsequently, the remaining segments were treated in a pulse-like fashion with 1 μg/ml CTX-K63 as described previously (Majoul et al. 1996, 1998), and were incubated at 37°C. At appropriate time points after the addition of the toxin, further segments of cells were removed and analyzed by spectrofluorimetry.

Preparation of CFP and YFP Expression Constructs

E. coli strain DH5α was used to amplify plasmid DNA. All CFP/YFP constructs were verified by DNA sequencing. For Vero cell transfections, endotoxin-free plasmid DNA was prepared from *E. coli* strain DH5α using the Endo-free Plasmid Maxi Kit (Qiagen). In-frame fusions of proteins of interest to cyan- or yellow-shifted GFP variants (ECFP or EYFP) were constructed either in the plasmids pECFP-C1 and pEYFP-C1 or pECFP-N1 and pEYFP-N1 (Clontech); these chimeras are thus expressed from the CMV promoter (for details and DNA accession numbers, see supplemental material).

Cell Culture, Cell Transfection, and Application of Cholera Toxin K63

Vero cells (African green monkey kidney cells; ECACC 84113001) were grown in phenol red-free DMEM with 2 mM glutamine, 10% FCS, 100 U/ml penicillin, and 0.1 mg/ml streptomycin at 10% CO_2 and 37°C. For transfection, cells were trypsinized, washed with PBS, and transferred into internal medium (100 mM potassium glutamate, 10 mM NaH_2PO_4, 5 mM magnesium acetate, 0.2 mM $CaCl_2$, 20 mM HEPES, 1 mM EGTA, 5 mM ATP, and vitamins A and E, 1 mM each). Cells were then electroporated twice (first pulse 0.25 kV, 175 μF, 15–20 msec; second pulse after 2 min 1.18 kV, 50 μF, 5–10 msec). The transfected cells were plated either onto 14.5 cm Petri dishes (for spectrofluorimetry) or onto coverslips in Petri dishes (for MMM experiments). Unless otherwise mentioned, cells were controlled for expression of GFP fusion proteins and cholera toxin binding 6 hr after transfection. For MMM experiments, cells were treated in a pulse-like manner with CTX-K63 (Majoul et al. 1996, 1998). CTX-K63 has no ADP-ribosylating activity due to a Ser63/Lys63 point mutation in the A subunit (Fontana et al., 1995). Following treatment with CTX-K63, cells remained in the CO_2 incubator until they were transferred to the thermostated microscope chamber.

Cy3 Labeling of CTX-K63

CTX-K-63 was equilibrated with 0.1 M bicine (pH 8.5) and incubated at 37°C in the presence of F_{ab} fragments of antibodies against the C-terminal KDEL signal of the A subunit and against the B subunit in order to protect the KDEL sequence and to reduce labeling of the B subunit in relation to the A subunit. The mixture was then incubated with about a 10-fold molar concentration of Cy3 (monosuccinimide ester) for 30 min. Following the removal of unbound Cy3 by gel filtration, bound F_{ab} fragments were dissociated by incubation in 0.1 M citrate (pH 3.5) and rapidly removed together with dissociated CTX-K63 subunits by centrifugal filtration through Centricon 50, followed by pH adjustment to 7.5. The ratio Cy3 × A subunit^{-1}/ Cy3 × B subunit^{-1} was >5 in the Cy3-CTX-K63 preparations used.

Trypsin Digestion of FCC III

Vero cells expressing FCC III were washed and equilibrated for 10 min on ice with various amounts of a stock solution containing 0.25 μg/μl activated streptolysin O. The appropriate amount of the toxin was evaluated from nuclear uptake of propidium iodide. Unbound streptolysin O was removed by washing with ice-cold equilibration

medium (120 mM potassium glutamate, 5 mM NaCl, and 5 mM $MgCl_2$). Subsequently, the temperature was raised to 37°C so that permeabilization occured and trypsin was added to a final concentration of 20 μg/ml in the absence or presence of 1% (v/v) Triton X-100. After 10 min, cells were washed with PBS containing 200 μg/ml soya bean trypsin inhibitor and scraped into Laemmli mix. Following SDS-PAGE (10% acrylamide), blots were probed with anti-GFP antibodies (Clontech) and antibodies directed against the cytoplasmic tail of p23.

Acknowledgments

We thank Drs. Paul Luzio, Gottfried Mieskes, Richard Premont, Margaret Robinson, and Irene Schulz for kindly providing plasmids, Dr. Mariagrazia Pizza for the generous gift of CTX-K63, and Mr. Hartmut Sebesse and other members of our repro-division for help with image processing. We thank Martin Dale (Cambridge) for expert technical assistance and Drs. Quentin Hanley, Reinhard Jahn, Paul Luzio, Walter Nickel, Jim Pawley, Margaret "Scottie" Robinson, and Karin Römisch for helpful comments on the manuscript. This work was supported by grants from the Deutsche Forschungsgemeinschaft (So 43/60-1 and He-1977-2) given to H.-D.S. and S.W.H., respectively and the Fond der Chemischen Industrie given to H.-D.S. R.D. is a Senior Research Fellow of the Wellcome Trust (047578).

Received October 30, 2000; revised May 30, 2001.

References

Aoe, T., Cukierman, E., Lee, A., Cassel, D., Peters, P.J., and Hsu, V.W. (1997). The KDEL receptor, ERD2, regulates intracellular traffic by recruiting a GTPase-activating protein for ARF1. EMBO J. *16*, 7305–7316.

Aoe, T., Lee, A.J., van Donselaar, E., Peters, P.J., and Hsu, V.W. (1998). Modulation of intracellular transport by transported proteins: insight from regulation of COPI-mediated transport. Proc. Natl. Acad. Sci. USA *95*, 1624–1629.

Barlowe, C. (2000). Traffic COPs of the early secretory pathway. Traffic *1*, 371–377.

Bewersdorf, J., Pick, R., and Hell, S.W. (1998). Multifocal multiphoton microscopy. Opt. Lett. *23*, 655–657.

Blum, R., Pfeiffer, F., Feick, P., Nastainczyk, W., Kohler, B., Schafer, K.H., and Schulz, I. (1999). Intracellular localization and in vivo trafficking of p24A and p23. J. Cell Sci. *112*, 537–548.

Bremser, M., Nickel, W., Schweikert, M., Ravazzola, M., Amherdt, M., Hughes, C.A., Sollner, T.H., Rothman, J.E., and Wieland, F.T. (1999). Coupling of coat assembly and vesicle budding to packaging of putative cargo receptors. Cell *96*, 495–506.

Bretscher, M.S., and Munro, S. (1993). Cholesterol and the Golgi apparatus. Science *261*, 1280–1281.

Cukierman, E., Huber, I., Rotman, M., and Cassel, D. (1995). The ARF1 GTPase-activating protein: zinc finger motif and Golgi complex localization. Science *270*, 1999–2002.

Dascher, C., and Balch, W.E. (1994). Dominant inhibitory mutants of ARF1 block endoplasmic reticulum to Golgi transport and trigger disassembly of the Golgi apparatus. J. Biol. Chem. *269*, 1437–1448.

Denk, W., and Svoboda, K. (1997). Photon upmanship: why multiphoton imaging is more than a gimmick. Neuron *18*, 351–357.

Denzel, A., Otto, F., Girod, A., Pepperkok, R., Watson, R., Rosewell, I., Bergeron, J.J., Solari, R.C., and Owen, M.J. (2000). The p24 family member p23 is required for early embryonic development. Curr. Biol. *10*, 55–58.

Dominguez, M., Dejgaard, K., Fullekrug, J., Dahan, S., Fazel, A., Paccaud, J.P., Thomas, D.Y., Bergeron, J.J., and Nilsson, T. (1998). gp25L/emp24/p24 protein family members of the cis-Golgi network bind both COP I and II coatomer. J. Cell Biol. *140*, 751–765.

Donaldson, J.G. and Jackson, C.L. (2000). Regulation and effectors of ARF GTPases. Curr. Opin. Cell Biol. *12*, 475–482.

Fiedler, K. and Rothman, J.E. (1997) Sorting determinants in the transmembrane domain of p24 proteins. J. Biol. Chem. *272*, 24739–24742.

Fiedler, K., Veit, M., Stamnes, M.A., and Rothman, J.E. (1996). Bimodal interaction of coatomer with the p24 family of putative cargo receptors. Science *273*, 1396–1399.

Fontana, M.R., Manetti, R., Giannelli, V., Magagnoli, C., Marchini, A., Olivieri, R., Domenighini, M., Rappuoli, R., and Pizza, M. (1995). Construction of nontoxic derivatives of cholera toxin and characterization of the immunological response against the A subunit. Infect. Immun. *63*, 2356–2360.

Füllekrug, J., Suganuma, T., Tang, B.L., Hong, W., Storrie, B., and Nilsson, T. (1999). Localization and recycling of gp27 (hp24γ3): complex formation with other p24 family members. Mol. Biol. Cell *10*, 1939–1955.

Gaynor, E.C., Graham, T.R., and Emr, S.D. (1998). COPI in ER/Golgi and intra-Golgi transport: do yeast COPI mutants point the way? Biochim. Biophys. Acta *1404*, 33–51.

Goldberg, J. (1999). Structural and functional analysis of the ARF1-ARFGAP complex reveals a role for coatomer in GTP hydrolysis. Cell *96*, 893–902.

Goldberg, J. (2000). Decoding of sorting signals by coatomer through a GTPase switch in the COPI coat complex. Cell *100*, 671–679.

Gommel, D., Orci, L., Emig, E.M., Hannah, M.J., Ravazzola, M., Nickel, W., Helms, J.B., Wieland, F.T., and Sohn, K. (1999). p24 and p23, the major transmembrane proteins of COPI-coated transport vesicles, form hetero-oligomeric complexes and cycle between the organelles of the early secretory pathway. FEBS Lett. *447*, 179–185.

Griffiths, G., Ericsson, M., Krijnse-Locker, J., Nilsson, T., Goud, B., Soling, H.D., Tang, B.L., Wong, S.H., and Hong, W. (1994). Localization of the Lys, Asp, Glu, Leu tetrapeptide receptor to the Golgi complex and the intermediate compartment in mammalian cells. J. Cell Biol. *127*, 1557–1574.

Hammond, C., and Helenius, A. (1995). Quality control in the secretory pathway. Curr. Opin. Cell Biol. *7*, 523–529.

Hsu, V.W., Shah, N., and Klausner, R.D. (1992). A brefeldin A-like phenotype is induced by the overexpression of a human ERD-2-like protein, ELP-1. Cell *69*, 625–635.

Kobayashi, T., Vischer, U.M., Rosnoblet, C., Lebrand, C., Lindsay, M., Parton, R.G., Kruithof, E.K., and Gruenberg, J. (2000). The tetraspanin CD63/lamp3 cycles between endocytic and secretory compartments in human endothelial cells. Mol. Biol. Cell *11*, 1829–1843.

Lanoix, J., Ouwendijk, J., Lin, C.C., Stark, A., Love, H.D., Ostermann, J., and Nilsson, T. (1999). GTP hydrolysis by arf-1 mediates sorting and concentration of Golgi resident enzymes into functional COP I vesicles. EMBO J. *18*, 4935–4948.

Letourneur, F., Gaynor, E.C., Hennecke, S., Demolliere, C., Duden, R., Emr, S.D., Riezman, H., and Cosson, P. (1994). Coatomer is essential for retrieval of dilysine-tagged proteins to the endoplasmic reticulum. Cell *79*, 1199–1207.

Lewis, B.A., and Engelman, D.M. (1983). Lipid bilayer thickness varies linearly with acyl chain length in fluid phosphatidylcholine vesicles. J. Mol. Biol. *166*, 211–217.

Lewis, M.J., and Pelham, H.R. (1992). Ligand-induced redistribution of a human KDEL receptor from the Golgi complex to the endoplasmic reticulum. Cell *68*, 353–364.

Lowe, M., and Kreis, T.E. (1996). In vivo assembly of coatomer, the COP-I coat precursor. J. Biol. Chem. *271*, 30725-30730.

Majoul, I.V., Bastiaens, P.I., and Soling, H.D. (1996). Transport of an external Lys-Asp-Glu-Leu (KDEL) protein from the plasma membrane to the endoplasmic reticulum: studies with cholera toxin in Vero cells. J. Cell Biol. *133*, 777–789.

Majoul, I., Sohn, K., Wieland, F.T., Pepperkok, R., Pizza, M., Hillemann, J., and Soling, H.D. (1998). KDEL receptor (Erd2p)-mediated retrograde transport of the cholera toxin A subunit from the Golgi involves COPI, p23, and the COOH terminus of Erd2p. J. Cell Biol. *143*, 601–612.

Malsam, J., Gommel, D., Wieland, F.T., and Nickel, W. (1999). A role

for ADP ribosylation factor in the control of cargo uptake during COPI-coated vesicle biogenesis. FEBS Lett. *462*, 267–272.

Marzioch, M., Henthorn, D.C., Herrmann, J.M., Wilson, R., Thomas, D.Y., Bergeron, J.J., Solari, R.C., and Rowley, A. (1999). Erp1p and Erp2p, partners for Emp24p and Erv25p in a yeast p24 complex. Mol. Biol. Cell *10*, 1923–1938.

Nickel, W., Sohn, K., Bunning, C., and Wieland, F.T. (1997). p23, a major COPI-vesicle membrane protein, constitutively cycles through the early secretory pathway. Proc. Natl. Acad. Sci. USA *94*, 11393–11398.

Nickel, W., Malsam, J., Gorgas, K., Ravazzola, M., Jenne, N., Helms, J.B. and Wieland, F.T. (1998). Uptake by COPI-coated vesicles of both anterograde and retrograde cargo is inhibited by GTPγS in vitro. J. Cell Sci. *111*, 3081–3090.

Orci, L., Stamnes, M., Ravazzola, M., Amherdt, M., Perrelet, A., Söllner, T.H., and Rothman, J.E. (1997). Bidirectional transport by distinct populations of COP I-coated vesicles. Cell *90*, 335–349.

Pelham, H.R.B. (1991). Recycling of proteins between the endoplasmic reticulum and Golgi complex. Curr. Opin. Cell Biol. *3*, 585–591.

Poon, P.P., Cassel, D., Spang, A., Rotman, M., Pick, E., Singer, R.A., and Johnston, G.C. (1999). Retrograde transport from the yeast Golgi is mediated by two ARF GAP proteins with overlapping function. EMBO J. *18*, 555–564.

Reinhard, C., Harter, C., Bremser, M., Brugger, B., Sohn, K., Helms, J.B., and Wieland, F. (1999). Receptor-induced polymerization of coatomer. Proc. Natl. Acad. Sci. USA *96*, 1224–1228.

Rothman, J.E., and Wieland, F.T. (1996). Protein sorting by transport vesicles. Science *272*, 227–234.

Semenza, J.C., Hardwick, K.G., Dean, N., and Pelham, H.R. (1990). ERD2, a yeast gene required for the receptor-mediated retrieval of luminal ER proteins from the secretory pathway. Cell *61*, 1349–1357.

Spang, A., Matsuoka, K., Hamamoto, S., Schekman, R., and Orci, L. (1998). Coatomer, Arf1p, and nucleotide are required to bud coat protein complex I-coated vesicles from large synthetic liposomes. Proc. Natl. Acad. Sci. USA *95*, 11199–11204.

Springer, S., Spang, A., and Schekman, R. (1999). A primer on vesicle budding. Cell *97*, 145–148.

Springer, S., Chen, E., Duden, R., Marzioch, M., Rowley, A., Hamamoto, S., Merchant, S., and Schekman, R. (2000). The p24 proteins are not essential for vesicular transport in *Saccharomyces cerevisiae*. Proc. Natl. Acad. Sci. USA *97*, 4034–4039.

Straub, M. and Hell, S.W. (1998). Fluorescence lifetime three-dimensional microscopy with picosecond precision using a multifocal multiphoton microscope. Appl. Phys. Lett. *73*, 1769–1771.

Straub, M., Lodemann, P., Holroyd, P., Jahn, R., and Hell, S.W. (2000). Live cell imaging by multifocal multiphoton microscopy. Eur. J. Cell Biol. *79*, 726–734.

Tanigawa, G., Orci, L., Amherdt, M., Ravazzola, M., Helms, J.B., and Rothman, J.E. (1993). Hydrolysis of bound GTP by ARF protein triggers uncoating of Golgi-derived COP-coated vesicles. J. Cell Biol. *123*, 1365–1371.

Townsley, F.M., Wilson, D.W., and Pelham, H.R. (1993). Mutational analysis of the human KDEL receptor: distinct structural requirements for Golgi retention, ligand binding and retrograde transport. EMBO J. *12*, 2821–2829.

Tsien, R.Y. (1998). The green fluorescent protein. Annu. Rev. Biochem. *67*, 509–544

Wieland, F., and Harter, C. (1999). Mechanisms of vesicle formation: insights from the COP system. Curr. Opin. Cell Biol. *11*, 440–446.